

IRRATIONAL-WINDOW-FILTER PROJECTION METHOD AND APPLICATION TO QUASIPERIODIC SCHRÖDINGER EIGENPROBLEMS *

KAI JIANG[†], XUEYANG LI[†], YAO MA[†], JUAN ZHANG[†], AND QI ZHOU[†]

Abstract. In this paper, we propose a new algorithm, the irrational-window-filter projection method (IWFP), for solving arbitrary dimensional global quasiperiodic systems. Based on the projection method (PM), IWFP further utilizes the concentrated distribution of Fourier coefficients to filter out relevant spectral points using an irrational window. Moreover, a corresponding index-shift transform is designed to make the Fast Fourier Transform available. The corresponding error analysis on the function approximation level is also given. We apply IWFP to 1D, 2D, and 3D quasiperiodic Schrödinger eigenproblems to demonstrate its accuracy and efficiency. IWFP exhibits a significant computational advantage over PM for both extended and localized quantum states. Furthermore, the widespread existence of such spectral point distribution feature can endow IWFP with significant potential for broader applications in quasiperiodic systems.

Key words. Irrational-window-filter projection method, Quasiperiodic Schrödinger eigenproblems, Extended state, Localized state, Convergence analysis.

AMS subject classifications. 35P05, 35J10, 65D15, 65T50, 81-08

1. Introduction. Quasiperiodic systems, as a natural extension of periodic structures, have been widely observed in physics and materials sciences, such as many-body problems, quasicrystals, incommensurate systems, polycrystalline materials, and quantum systems [28, 31, 8, 36, 14]. Over time, a growing realization has emerged that underlying irrational numbers of quasiperiodic systems impart various fascinating features [27, 25, 5, 7]. Particularly, in quantum systems, numerous intriguing physical phenomena have been discovered to be closely related to quasiperiodic structures, including quantum Hall effect, Anderson localization, topological insulators, and mobility edge [37, 15, 14, 30, 38].

Quasiperiodic systems pose significant challenges for numerical simulations, due to their space-filling order without decay or translation invariance. Recently years, several methods for solving quasiperiodic systems have been developed. The widely used periodic approximation method [42] employs periodic solutions to approximate quasiperiodic solutions, inevitably introducing rational approximation errors [16, 17, 18]. A more accurate algorithm is the projection method (PM), which treats each quasiperiodic system as an irrational manifold of a high-dimensional periodic system [16]. PM has been proven to possess high accuracy within the quasiperiodic function space, and is efficient owing to its utilization of fast Fourier transform (FFT) to reduce computational complexity [20].

Motivation. PM has shown outstanding advantages in accurately computing quasiperiodic systems, especially in incommensurate quantum field [20, 24, 41, 10, 19, 43]. However, when using PM, quasiperiodic function after lifting dimension may exhibit distinct regularities along different directions, leading to a notable deterioration in convergence. This flaw becomes apparent when solving some quasiperiodic systems

*Submitted to xxx.

[†] Hunan Key Laboratory for Computation and Simulation in Science and Engineering, Key Laboratory of Intelligent Computing and Information Processing of Ministry of Education, School of Mathematics and Computational Science, Xiangtan University, Xiangtan, Hunan, China, 411105. (kaijiang@xtu.edu.cn, lixy1217@xtu.edu.cn, mayao@smail.xtu.edu.cn, zhangjuan@xtu.edu.cn, qizhou@smail.xtu.edu.cn).

with unusual solution features.

Focusing on Anderson localization, the phenomenon of wave diffusion being absent in disordered or quasiperiodic medium, it is of great significance in regulating various physical properties in materials, including conductivity, optical properties, and magnetism [1]. Over the past few decades, incommensurate electrical structures, drawing attention for their capacity of achieving the continuous transition from extended state to localized state, have been experimentally studied through techniques like cold atom control and optical superlattice [29, 9, 35, 39]. Under the tight-binding limit, the Hamiltonian of incommensurate quantum system can be mapped onto the well-known almost Mathieu operator, which is a typical form of quasiperiodic Schrödinger operators [33]. Since the 1980s, substantial progress has been made in the spectral theory of quasiperiodic Schrödinger operators. Researchers have found that the spectral structure of the Schrödinger operator can be decomposed into pure point, singular continuous, and absolutely continuous spectra, which correspond to localized, critical, and extended states of quantum systems, respectively [33, 2, 3, 4, 12]. While significant theoretical works have been conducted on one-dimensional cases of QSEs, addressing two- and higher-dimensional scenarios remains a challenging endeavor.

When numerically solving arbitrary dimensional quasiperiodic Schrödinger eigenproblems (QSEs), especially in cases where the wavefunction exhibits localization, PM becomes inefficient due to the huge computational cost. Based on PM, several inspiring works have been introduced. Among these, a reciprocal space sampling method based on PM has been proposed to characterize the density of states of QSE [40]. A reduced PM has been developed to improve the condition number of discretize QSE [11]. However, these algorithms do not essentially improve the computational efficiency of PM and are incapable of addressing localized problems. How to develop PM to high efficiently solve QSEs is the main purpose of this paper.

Contribution. In this paper, we propose a new algorithm, named the *irrational-window-filter projection method* (IWFPMP), for solving arbitrary dimensional global quasiperiodic systems. Based on the projection method, IWFPMP further utilizes the concentrated distribution of Fourier coefficients to filter out relevant spectral points using an irrational window. Moreover, a corresponding index-shift transform is designed to make the FFT available. The corresponding error analysis on the function approximation level is also given. We apply IWFPMP to 1D, 2D, and 3D QSEs to demonstrate its accuracy and efficiency. An efficient diagonal preconditioner is also designed for the discrete QSEs to significantly reduce condition number. Numerous experiments demonstrate that IWFPMP has an absolute computational advantage over PM for both extended and localized quantum states.

Organization. The article is structured as follows. In [section 2](#), we introduce the preliminaries about quasiperiodic functions and give a brief introduction of PM. In [section 3](#), we present the design concept of IWFPMP and detail its implementation process. Moreover, we define a new norm in quasiperiodic function space to enable the convergence analysis of our method. In [section 4](#), we illustrate the effectiveness and superiority of IWFPMP through its application to various QSEs. Finally, in [section 5](#), we carry out the summary of this paper and give an outlook of future work.

2. Quasiperiodic functions and projection method (PM). In this section, we present some preliminaries about quasiperiodic functions and offer a brief overview of PM.

DEFINITION 2.1. A matrix $\mathbf{P} \in \mathbb{R}^{d \times n}$ is called the *projection matrix*, if it belongs to the set $\mathbb{P}^{d \times n} := \{\mathbf{P} = (\mathbf{p}_1, \dots, \mathbf{p}_n) \in \mathbb{R}^{d \times n} : \mathbf{p}_1, \dots, \mathbf{p}_n \text{ are } \mathbb{Q}\text{-linearly independent,}$

$\text{rank}(\mathbf{P}) = d\}$.

DEFINITION 2.2. A d -dimensional function $u(\mathbf{x})$ is quasiperiodic if there exists a continuous n -dimensional periodic function $U(\mathbf{y})$ and a projection matrix $\mathbf{P} \in \mathbb{P}^{d \times n}$, such that $u(\mathbf{x}) = U(\mathbf{P}^T \mathbf{x})$, for all $\mathbf{x} \in \mathbb{R}^d$.

REMARK 2.1. The periodic function $U(\mathbf{y})$ is called the parent function of $u(\mathbf{x})$. And we use the notation $\mathcal{Q}(\mathbb{R}^d)$ to represent the set of all d -dimensional quasiperiodic functions. Without loss of generality, we always assume that all parent functions are measurable on n -dimensional torus $\mathbb{T}^n := (\mathbb{R}/2\pi\mathbb{Z})^n$.

For n -dimensional periodic functions U and V , their inner product is

$$\langle U, V \rangle := \frac{1}{(2\pi)^n} \int_{[0, 2\pi]^n} U(\mathbf{y}) \bar{V}(\mathbf{y}) d\mathbf{y}.$$

We say $U \in \mathcal{L}^2(\mathbb{T}^n)$ if $\|U\|_{\mathcal{L}^2} := \langle U, U \rangle^{1/2} < +\infty$. Denote Fourier basis function $\varphi_{\mathbf{k}}(\mathbf{y}) := e^{i\mathbf{k} \cdot \mathbf{y}}$ for index $\mathbf{k} \in \mathbb{Z}^n$, where $\mathbf{k} \cdot \mathbf{y} = \sum_{j=1}^n k_j y_j$. It is obvious that for any $\mathbf{k}, \mathbf{k}' \in \mathbb{Z}^d$, the Fourier basis functions $\varphi_{\mathbf{k}}$ and $\varphi_{\mathbf{k}'}$ are orthogonal, i.e.

$$\langle \varphi_{\mathbf{k}}, \varphi_{\mathbf{k}'} \rangle := \delta_{\mathbf{k}\mathbf{k}'} = \begin{cases} 1, & \mathbf{k} = \mathbf{k}', \\ 0, & \mathbf{k} \neq \mathbf{k}'. \end{cases}$$

Then, for a periodic function $U \in \mathcal{L}^2(\mathbb{T}^n)$, its Fourier series is defined by

$$U(\mathbf{y}) = \sum_{\mathbf{k} \in \mathbb{Z}^n} \hat{U}_{\mathbf{k}} \varphi_{\mathbf{k}}(\mathbf{y}), \quad \hat{U}_{\mathbf{k}} := \langle U, \varphi_{\mathbf{k}} \rangle.$$

For a quasiperiodic function $u(\mathbf{x}) \in \mathcal{Q}(\mathbb{R}^d)$, its mean value $M(u)$ is defined as

$$M(u) := \lim_{T \rightarrow +\infty} \frac{1}{(2T)^d} \int_{\mathbf{s} + [-T, T]^d} u(\mathbf{x}) d\mathbf{x}, \quad \forall \mathbf{s} \in \mathbb{R}^d.$$

Correspondingly, the inner product and norm of $u, v \in \mathcal{Q}(\mathbb{R}^d)$ can be defined as

$$\langle u, v \rangle := M(u\bar{v}), \quad \|u\| := (M(|u|^2))^{1/2}.$$

We say $u \in \mathcal{L}_{\mathcal{Q}}^2$ if $\|u\| < +\infty$. Note that the definition of Fourier basis functions can be easily extended to more general cases as $\varphi_{\mathbf{q}}(\mathbf{x}) := e^{i\mathbf{q} \cdot \mathbf{x}}$, for any $\mathbf{q}, \mathbf{x} \in \mathbb{R}^d$. Then, the Fourier-Bohr transform of u is $\hat{u}_{\mathbf{q}} := M(u\varphi_{\mathbf{q}})$, $\mathbf{q} \in \mathbb{R}^d$.

LEMMA 2.3 ([20], Theorem 4.1). For a d -dimensional quasiperiodic function u and its associated parent function U , it holds $\hat{u}_{\mathbf{q}} = \hat{U}_{\mathbf{k}}$ when $\mathbf{q} = \mathbf{P}\mathbf{k}$.

Then the generalized Fourier series of $u(\mathbf{x}) \in \mathcal{L}_{\mathcal{Q}}^2$ is given by

$$u(\mathbf{x}) = \sum_{\mathbf{k} \in \mathbb{Z}^n} \hat{U}_{\mathbf{k}} \varphi_{\mathbf{P}\mathbf{k}}(\mathbf{x}).$$

REMARK 2.2. When the parent function satisfies certain regularity condition, all Fourier coefficients have a common decay property. Specifically, if $U \in \mathcal{H}^\alpha(\mathbb{T}^n)$, there exists a positive constant C such that $\hat{U}_{\mathbf{k}} \leq C|\mathbf{P}\mathbf{k}|^{-\alpha}|U|_{\mathcal{H}^\alpha}$ [13]. Here, the definitions of seminorm $|\cdot|_{\mathcal{H}^\alpha}$ and the corresponding Sobolev space $\mathcal{H}^\alpha(\mathbb{T}^n)$ are given in (3.12).

Next, we briefly introduce the PM. Different from previous numerical methods, PM grasps the essential feature of a d -dimensional quasiperiodic function that can be embedded into its associated n -dimensional parent periodic function [16]. As a result, PM computes the n -dimensional parent periodic system in a pseudospectral way instead of directly addressing quasiperiodic system. Then, PM projects these results onto d -dimensional space by the projection matrix \mathbf{P} to obtain quasiperiodic system. Concretely, given a positive integer N , we define the finite index set

$$\mathcal{K}_N := \{\mathbf{k} \in \mathbb{Z}^n : \mathbf{k} \in [-N, N]^n\}.$$

Then, the dual grid of \mathcal{K}_N is given by

$$\mathcal{G}_N := \{\mathbf{y}_\ell = \pi\ell/N \in [0, 2\pi)^n : \ell \in \mathbb{Z}^n \cap [0, 2N)^n\}.$$

For periodic grid functions $U, V \in \mathcal{G}_N$, the discrete inner product is

$$\langle U, V \rangle_N := \frac{1}{(2N)^n} \sum_{\mathbf{y}_\ell \in \mathcal{G}_N} U(\mathbf{y}_\ell) \overline{V(\mathbf{y}_\ell)}.$$

Limit the space $\mathcal{L}^2(\mathbb{T}^n)$ to a finite dimensional subspace spanned by the $\{\varphi_{\mathbf{k}} : \mathbf{k} \in \mathcal{K}_N\}$, we obtain the discrete Fourier-Bohr series of $u \in \mathcal{L}_Q^2$ [20]

$$u(\mathbf{x}) = \sum_{\mathbf{k} \in \mathcal{K}_N} \bar{U}_{\mathbf{k}} \varphi_{\mathbf{P}\mathbf{k}}(\mathbf{x}), \quad \bar{U}_{\mathbf{k}} := \langle U, \varphi_{\mathbf{k}} \rangle_N.$$

The corresponding error analysis of PM can refer to [20]. Moreover, since discrete Fourier coefficients originate from the periodic parent function, PM can use the n -dimensional FFT to improve computing efficiency.

3. Irrational-window-filter projection method (IWFPM). When using PM to address some quasiperiodic systems, such as quasiperiodic Schrödinger eigenproblems, an interesting phenomenon has been observed that the Fourier coefficients are concentrated in a narrow elongated area (see [40, 11]). Moreover, the tilt angle of this area is associated with the projection matrix. Here, we develop PM to the case of concentrated Fourier coefficients.

3.1. Irrational window. Based on the decay property of Fourier coefficients mentioned in Remark 2.2, we discover that Fourier coefficients are concentrated in a hyperparallelogram area along the $\mathbf{P}\mathbf{k} = 0$ direction. Further, we divide $\mathbf{P} = (\mathbf{P}_I, \mathbf{P}_{II})$, where $\mathbf{P}_I \in \mathbb{R}^{d \times d}$ and $\mathbf{P}_{II} \in \mathbb{R}^{d \times (n-d)}$. According to the definition of projection matrix, we can always make the d -order matrix \mathbf{P}_I invertible. Hence, there exists an elementary row transform \mathbf{P}_I^{-1} such that $\mathbf{P}_I^{-1}\mathbf{P} = (\mathbf{I}_d, \mathbf{Q})$, where \mathbf{I}_d is the d -order identity matrix and $\mathbf{Q} := \mathbf{P}_I^{-1}\mathbf{P}_{II} \in \mathbb{R}^{d \times (n-d)}$. Through this transform, we can concentrate all irrational numbers in \mathbf{P} into \mathbf{Q} . Correspondingly, we partition the index $\mathbf{k} \in \mathbb{R}^n$ into two parts: $\mathbf{k} = (\mathbf{k}_I, \mathbf{k}_{II})^T$, $\mathbf{k}_I \in \mathbb{R}^d$, $\mathbf{k}_{II} \in \mathbb{R}^{n-d}$. Then, the hyperparallelogram tilt along the $\mathbf{P}\mathbf{k} = \mathbf{k}_I + \mathbf{Q}\mathbf{k}_{II} = 0$ direction.

Based on this distribution feature of Fourier coefficients, we can define an irrational window for given two positive integers K and L as

$$\mathcal{W}_{K,L} := \{\mathbf{k} = (\mathbf{k}_I, \mathbf{k}_{II})^T \in \mathbb{R}^n : \mathbf{k}_{II} \in [-L, L]^{n-d}, \mathbf{k}_I + \mathbf{Q}\mathbf{k}_{II} \in [-K, K]^d\}.$$

Obviously, irrational window $\mathcal{W}_{K,L}$ is determined by the irrational numbers in the projection matrix \mathbf{P} . Then, we can define a hyperparallelogram index set

$$(3.1) \quad \mathcal{K}_{K,L} := \mathcal{W}_{K,L} \cap \mathbb{Z}^n.$$

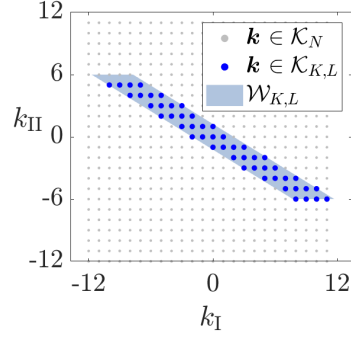


Fig. 1: Rectangle index set \mathcal{K}_N , parallelogram index set $\mathcal{K}_{K,L}$, and irrational window $\mathcal{W}_{K,L}$ when $d = 1$, $n = 2$, $N = 12$, $K = 2$, $L = 6$, $\mathbf{P} = (1, (\sqrt{5} + 1)/2)$.

As an illustrated example, Figure 1 presents the rectangle index set \mathcal{K}_N , parallelogram index set $\mathcal{K}_{K,L}$, and irrational window $\mathcal{W}_{K,L}$ when $d = 1$, $n = 2$, $N = 12$, $K = 2$, $L = 6$ for projection matrix $\mathbf{P} = (1, (\sqrt{5} + 1)/2)$. We can observe that using the index set \mathcal{K}_N of PM would require $2N \times 2N = 576$ indicators, while using $\mathcal{K}_{K,L}$ significantly reduces this number to $2K \times 2L = 48$.

3.2. Index-shift map. For the Fourier coefficient index set $\mathcal{K}_{K,L}$, there seems a drawback in practical calculations that the irregular shape may make the FFT inapplicable. To address this issue, we introduce an index-shift map ϱ , defined by

$$\varrho(\mathbf{k}) = \mathbf{k}^* = (k_j^*)_{j=1}^n,$$

where

$$(3.2) \quad k_j^* = \begin{cases} k_j \bmod 2K, & \text{if } j = 1, \dots, d, \\ k_j \bmod 2L, & \text{if } j = d + 1, \dots, n. \end{cases}$$

Here, “mod” represents modulo operation.

Apply ϱ to all indicators of $\mathcal{K}_{K,L}$, we can obtain the following hyperrectangle index set

$$\mathcal{K}_{K,L}^* := \{\mathbf{k} = (\mathbf{k}_I, \mathbf{k}_{II})^T \in \mathbb{Z}^n : \mathbf{k}_I \in [0, 2K)^d, \mathbf{k}_{II} \in [0, 2L)^{n-d}\}.$$

Correspondingly, the set of dual grid points can be defined as

$$\mathcal{G}_{K,L} := \{\mathbf{y}_\ell = (\pi\ell_1/K, \pi\ell_2/L)^T \in [0, 2\pi)^n : \ell = (\ell_1, \ell_2) \in \mathcal{K}_{K,L}^*\}.$$

Obviously,

$$(3.3) \quad \varphi_{\mathbf{k}}(\mathbf{y}_\ell) = \varphi_{\mathbf{k}^*}(\mathbf{y}_\ell), \quad \forall \mathbf{y}_\ell \in \mathcal{G}_{K,L}, \mathbf{k} \in \mathcal{K}_{K,L}.$$

REMARK 3.1. Based on the equivalence (3.3), we can establish the connection between the discrete Fourier transforms on indicator set $\mathcal{K}_{K,L}$ and indicator set $\mathcal{K}_{K,L}^*$ in Subsection 3.3.

As an example, Figure 2 illustrates the operation of the index-shift map on the index set $\mathcal{K}_{K,L}$. It shows the parallelogram index set $\mathcal{K}_{K,L}$, the rectangle index set $\mathcal{K}_{K,L}^*$, and the grid points $\mathcal{G}_{K,L}$ when $d = 1$, $n = 2$, $K = 2$, $L = 6$, $\mathbf{P} = (1, (\sqrt{5} + 1)/2)$.

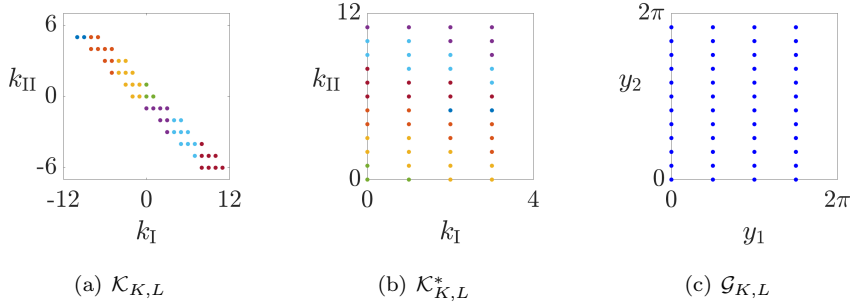


Fig. 2: The parallelogram index set $\mathcal{K}_{K,L}$ (left), the rectangle index set $\mathcal{K}_{K,L}^*$ (middle), and the grid points $\mathcal{G}_{K,L}$ (right) when $d = 1$, $n = 2$, $K = 2$, $L = 6$, $\mathbf{P} = (1, (\sqrt{5}+1)/2)$.

Although ϱ is a bijection, the calculation of the inverse of ϱ cannot be directly reflected by (3.2). Hence, we attempt to give the mathematical expression of ϱ^{-1} in the following. Let $(\mathbf{Q}\mathbf{k}_{\text{II}})_j$ denotes the j th component of the vector $\mathbf{Q}\mathbf{k}_{\text{II}}$. According to the definition of the part $\mathbf{k}_{\text{I}} = (k_j)_{j=1}^d$ in index $\mathbf{k} \in \mathcal{K}_{K,L}$, it is obvious that the value range of k_j is the $2K$ integers within the interval $[-K - (\mathbf{Q}\mathbf{k}_{\text{II}})_j, K - (\mathbf{Q}\mathbf{k}_{\text{II}})_j]$. Among these integers, only one can be divisible by $2K$, and that is $R_j = \lceil (-K - (\mathbf{Q}\mathbf{k}_{\text{II}})_j)/2K \rceil \cdot 2K$, where $\lceil \cdot \rceil$ represents rounding up. Then, the computation of the inverse map

$$(3.4) \quad \varrho^{-1}(\mathbf{k}^*) = \mathbf{k} = (\mathbf{k}_{\text{I}}, \mathbf{k}_{\text{II}}), \quad \mathbf{k}^* \in \mathcal{K}_{K,L}^*$$

is given by two steps. The first step is to compute \mathbf{k}_{II} as following

$$(3.5) \quad k_j = \begin{cases} k_j^*, & \text{if } k_j^* < L, \\ k_j^* - 2L, & \text{if } L \leq k_j^* < 2L, \end{cases} \quad j = d+1, \dots, n,$$

and the second step is to compute \mathbf{k}_{I} as following

$$(3.6) \quad k_j = \begin{cases} k_j^* + R_j, & \text{if } k_j^* + R_j + (\mathbf{Q}\mathbf{k}_{\text{II}})_j < K, \\ k_j^* + R_j - 2K, & \text{otherwise,} \end{cases} \quad j = 1, \dots, d.$$

3.3. Implementation. Based on the new index set $\mathcal{K}_{K,L}$ and the index-shift map ϱ introduced in the previous two subsections, we can now detail the whole process of IWFP.

For n -dimensional periodic functions U and V , the discrete inner product over $\mathcal{G}_{K,L}$ is defined by

$$(3.7) \quad \langle U, V \rangle_{K,L} := \frac{1}{2^n K^d L^{n-d}} \sum_{\mathbf{y}_{\ell} \in \mathcal{G}_{K,L}} U(\mathbf{y}_{\ell}) \overline{V(\mathbf{y}_{\ell})}.$$

Additionally, we define a finite dimensional subspace of $\mathcal{L}^2(\mathbb{T}^n)$ as $\mathcal{S}_{K,L} := \text{span}\{\varphi_{\mathbf{k}} : \mathbf{k} \in \mathcal{K}_{K,L}\}$. Then, the Fourier interpolation operator of IWFP is defined by

$$(3.8) \quad \begin{aligned} \mathcal{I}_{K,L} : \mathcal{L}_Q^2 &\rightarrow \mathcal{S}_{K,L}, \\ u(\mathbf{x}) &\mapsto \sum_{\mathbf{k} \in \mathcal{K}_{K,L}} \tilde{U}_{\mathbf{k}} \varphi_{\mathbf{P}\mathbf{k}}(\mathbf{x}), \end{aligned}$$

where $\tilde{U}_{\mathbf{k}} := \langle U, \varphi_{\mathbf{k}} \rangle_{K,L}$.

Denote $\mathbf{U} := (U(\mathbf{y}_{\ell}))_{\mathbf{y}_{\ell} \in \mathcal{G}_{K,L}}$, then there is a discrete Fourier transform \mathbf{F} equivalent to $\mathcal{I}_{K,L}$ such that

$$(3.9) \quad \tilde{\mathbf{U}} = \mathbf{F}\mathbf{U}, \quad \tilde{\mathbf{U}} := (\tilde{U}_{\mathbf{k}})_{\mathbf{k} \in \mathcal{K}_{K,L}}.$$

Correspondingly, let \mathbf{F}^* be the standard discrete Fourier transform, i.e.

$$(3.10) \quad \tilde{\mathbf{U}}^* = \mathbf{F}^*\mathbf{U}, \quad \tilde{\mathbf{U}}^* := (\tilde{U}_{\mathbf{k}^*}^*)_{\mathbf{k}^* \in \mathcal{K}_{K,L}^*},$$

where $\tilde{U}_{\mathbf{k}^*}^* := \langle U, \varphi_{\mathbf{k}^*} \rangle_{K,L}$. Based on [Subsection 3.2](#), we can define the index-shift transform \mathbf{T} with respect to the inverse map ϱ^{-1} such that $\tilde{\mathbf{U}} = \mathbf{T}\tilde{\mathbf{U}}^*$. Therefore, to implement the discrete Fourier transform \mathbf{F} , we can equivalently apply the transform \mathbf{F}^* and \mathbf{T}^* successively. In other words, it means that $\mathbf{F} = \mathbf{T}\mathbf{F}^*$.

REMARK 3.2. *It is worth emphasizing the purpose of this transformation is to ensure that the FFT can still be applied to efficiently obtain the required Fourier coefficients.*

[Algorithm 3.1](#) summarizes the implementation steps of IWFPM.

Algorithm 3.1 Irrational-window-filter projection method

Require: projection matrix \mathbf{P} , size of index set: K and L

- 1: Generate index sets $\mathcal{K}_{K,L}$ and $\mathcal{K}_{K,L}^*$
 - 2: Obtain $\tilde{\mathbf{U}}^* = (\tilde{U}_{\mathbf{k}^*}^*)_{\mathbf{k}^* \in \mathcal{K}_{K,L}^*}$ by solving [\(3.10\)](#) using FFT
 - 3: **for** $\mathbf{k}^* \in \mathcal{K}_{K,L}^*$ **do**
 - 4: Solve $\tilde{\mathbf{k}} = \varrho^{-1}(\mathbf{k}^*)$ according to [\(3.4\)](#)-[\(3.6\)](#)
 - 5: Store $\tilde{U}_{\tilde{\mathbf{k}}} = \tilde{U}_{\mathbf{k}^*}^*$
 - 6: **end for**
 - 7: Calculate the Fourier interpolation result $u = \sum_{\mathbf{k} \in \mathcal{K}_{K,L}} \tilde{U}_{\mathbf{k}} \varphi_{\mathbf{P}\mathbf{k}}$
-

REMARK 3.3. *Note that the index-shift operator \mathbf{T} only modifies the indicators of Fourier coefficients without changing the value. Thus, the computational cost of the discrete Fourier transform \mathbf{F} corresponding to IWFPM is entirely equivalent to that of the standard discrete Fourier transform \mathbf{F}^* . Further, by utilizing FFT, the computational cost of \mathbf{F} is of order $O(K^d L^{n-d}(\log K + \log L))$.*

3.4. Error analysis. In this subsection, we give an error analysis of IWFPM. For simplicity of analysis, we use the notation $A[u] \lesssim B[u]$, which means that there exists a positive constant satisfying $A[u] \leq CB[u]$, where $A[u]$ and $B[u]$ are functional with respect to $u(\mathbf{x})$, and the positive constant C is independent of K , L , and any norm of u . Moreover, we abbreviate $A[u] \lesssim B[u]$ and $B[u] \lesssim A[u]$ as $A[u] \simeq B[u]$. The Sobolev seminorm and norm of quasiperiodic function $u \in \mathcal{L}_{\mathbf{Q}}^2$ for any $\alpha \geq 0$ are defined as

$$(3.11) \quad \begin{aligned} |u|_{\alpha} &:= \left(\sum_{\mathbf{k} \in \mathbb{Z}^n} \|\mathbf{P}\mathbf{k}\|^{2\alpha} |\hat{U}_{\mathbf{k}}|^2 \right)^{1/2}, \\ \|u\|_{\alpha} &:= \left(\sum_{\mathbf{k} \in \mathbb{Z}^n} (1 + \|\mathbf{P}\mathbf{k}\|^{2\alpha}) |\hat{U}_{\mathbf{k}}|^2 \right)^{1/2}. \end{aligned}$$

Here we set $0^0 = 1$. And we say $u \in \mathcal{H}_Q^\alpha$ if $\|u\|_\alpha < +\infty$. The Sobolev seminorm and norm of periodic function $U \in \mathcal{L}^2(\mathbb{T}^n)$ for any $\alpha \geq 0$ are defined as

$$(3.12) \quad \begin{aligned} |U|_{\mathcal{H}^\alpha} &:= \left(\sum_{\mathbf{k} \in \mathbb{Z}^n} \|\mathbf{k}\|^{2\alpha} |\hat{U}_{\mathbf{k}}|^2 \right)^{1/2}, \\ \|U\|_{\mathcal{H}^\alpha} &:= \left(\sum_{\mathbf{k} \in \mathbb{Z}^n} (1 + \|\mathbf{k}\|^{2\alpha}) |\hat{U}_{\mathbf{k}}|^2 \right)^{1/2}. \end{aligned}$$

And we say $U \in \mathcal{H}^\alpha(\mathbb{T}^n)$ if $\|U\|_{\mathcal{H}^\alpha} < +\infty$. If the norm of the projection matrix \mathbf{P} is not very large, the quasiperiodic norm $\|u\|_\alpha$ can be effectively controlled by the periodic norm $\|U\|_{\mathcal{H}^\alpha}$, while the opposite is not true. $u \in \mathcal{H}_Q^\alpha$ may not necessarily lead to $U \in \mathcal{H}^\alpha(\mathbb{T}^n)$, or the norm $\|U\|_{\mathcal{H}^\alpha}$ may be much larger than the norm $\|u\|_\alpha$. Considering the definition of index set $\mathcal{K}_{K,L}$ (3.1), we adopt a new norm definition

$$(3.13) \quad \begin{aligned} |u|_{\alpha,\beta} &:= \left(\sum_{\mathbf{k} \in \mathbb{Z}^n} (\|\mathbf{k}_I + \mathbf{Q}\mathbf{k}_{II}\|^{2\alpha} + \|\mathbf{k}_{II}\|^{2\beta}) |\hat{U}_{\mathbf{k}}|^2 \right)^{1/2}, \\ \|u\|_{\alpha,\beta} &:= \left(\sum_{\mathbf{k} \in \mathbb{Z}^n} (1 + \|\mathbf{k}_I + \mathbf{Q}\mathbf{k}_{II}\|^{2\alpha} + \|\mathbf{k}_{II}\|^{2\beta}) |\hat{U}_{\mathbf{k}}|^2 \right)^{1/2}, \end{aligned}$$

for any $\alpha, \beta \geq 0$. Note that the Cauchy-Schwarz inequality can lead to

$$\begin{aligned} \left(\sum_{\mathbf{k} \in \mathbb{Z}^n} \lambda_{\mathbf{k}}^2 |\hat{U}_{\mathbf{k}} + \hat{V}_{\mathbf{k}}|^2 \right)^{1/2} &\leq \left(\sum_{\mathbf{k} \in \mathbb{Z}^n} \lambda_{\mathbf{k}}^2 (|\hat{U}_{\mathbf{k}}|^2 + |\hat{V}_{\mathbf{k}}|^2) + 2 \sum_{\mathbf{k} \in \mathbb{Z}^n} \lambda_{\mathbf{k}}^2 |\hat{U}_{\mathbf{k}} \hat{V}_{\mathbf{k}}| \right)^{1/2} \\ &\leq \left(\sum_{\mathbf{k} \in \mathbb{Z}^n} \lambda_{\mathbf{k}}^2 (|\hat{U}_{\mathbf{k}}|^2 + |\hat{V}_{\mathbf{k}}|^2) + 2 \left(\sum_{\mathbf{k} \in \mathbb{Z}^n} \lambda_{\mathbf{k}}^2 |\hat{U}_{\mathbf{k}}|^2 \sum_{\mathbf{k} \in \mathbb{Z}^n} \lambda_{\mathbf{k}}^2 |\hat{V}_{\mathbf{k}}|^2 \right)^{1/2} \right)^{1/2} \\ &= \left(\sum_{\mathbf{k} \in \mathbb{Z}^n} \lambda_{\mathbf{k}}^2 |\hat{U}_{\mathbf{k}}|^2 \right)^{1/2} + \left(\sum_{\mathbf{k} \in \mathbb{Z}^n} \lambda_{\mathbf{k}}^2 |\hat{V}_{\mathbf{k}}|^2 \right)^{1/2} \end{aligned}$$

for any real sequence $\{\lambda_{\mathbf{k}}\}_{\mathbf{k} \in \mathbb{Z}^n}$. Therefore, it is easy to prove that $|\cdot|_{\alpha,\beta}$ and $\|u\|_{\alpha,\beta}$ satisfy the conditions for defining the seminorms and the norm, respectively. Here we say $u \in \mathcal{H}_Q^{\alpha,\beta}$ if $\|u\|_{\alpha,\beta} < +\infty$.

Then we give the following lemma to show the relation between the above three spaces.

LEMMA 3.1. *Suppose that $\alpha \geq \beta \geq 0$, then $u \in \mathcal{H}_Q^{\alpha,\beta}$ if and only if $u \in \mathcal{H}_Q^\alpha$ and $U \in \mathcal{H}^\beta(\mathbb{T}^n)$, i.e. the seminorms and norms defined in (3.11), (3.12) and (3.13) satisfy*

$$\begin{aligned} |u|_{\alpha,\beta} &\simeq |u|_\alpha + |U|_{\mathcal{H}^\beta}, \\ \|u\|_{\alpha,\beta} &\simeq \|u\|_\alpha + \|U\|_{\mathcal{H}^\beta}. \end{aligned}$$

Proof. The proof is in Appendix A. □

The truncation approximation operator can be defined via the following projection operator

$$(3.14) \quad \begin{aligned} \mathcal{P}_{K,L} : \mathcal{L}_Q^2 &\rightarrow \mathcal{S}_{K,L} \\ u &\mapsto \sum_{\mathbf{k} \in \mathcal{K}_{K,L}} \hat{U}_{\mathbf{k}} \varphi_{\mathbf{P}\mathbf{k}}, \end{aligned}$$

where $\hat{U}_{\mathbf{k}}$ is the Fourier coefficient for $\mathbf{k} \in \mathcal{K}_{K,L}$.

LEMMA 3.2. Suppose that $u \in \mathcal{H}_{\mathcal{Q}}^{\alpha,\beta}$ with $\alpha \geq \beta \geq 0$, then the error of truncation approximation $\mathcal{P}_{K,L}$ (3.14) satisfies

$$\begin{aligned} |u - \mathcal{P}_{K,L}u|_{\mu,\nu} &\lesssim K^{-\alpha}(K^\mu + L^\nu)|u|_\alpha + L^{-\beta}(K^\mu + L^\nu)|U|_{\mathcal{H}^\beta}, \\ \|u - \mathcal{P}_{K,L}u\|_{\mu,\nu} &\lesssim K^{-\alpha}(K^\mu + L^\nu)\|u\|_\alpha + L^{-\beta}(K^\mu + L^\nu)\|U\|_{\mathcal{H}^\beta}, \end{aligned}$$

for $\mu \in [0, \alpha]$, $\nu \in [0, \beta]$.

Proof. The proof is in Appendix B. \square

Combined Lemma 3.2 with Lemma 3.1, the following corollary can be easily obtained.

COROLLARY 3.3. Suppose that $u \in \mathcal{H}_{\mathcal{Q}}^{\alpha,\beta}$ with $\alpha \geq \beta \geq 0$, then the error of truncation approximation $\mathcal{P}_{K,L}$ (3.14) satisfies

$$\begin{aligned} |u - \mathcal{P}_{K,L}u|_{\mu,\nu} &\lesssim (K^{-\alpha} + L^{-\beta})(K^\mu + L^\nu)|u|_{\alpha,\beta}, \\ \|u - \mathcal{P}_{K,L}u\|_{\mu,\nu} &\lesssim (K^{-\alpha} + L^{-\beta})(K^\mu + L^\nu)\|u\|_{\alpha,\beta}, \end{aligned}$$

for $\mu \in [0, \alpha]$, $\nu \in [0, \beta]$.

THEOREM 3.4. Suppose that $u \in \mathcal{H}_{\mathcal{Q}}^{\alpha,\beta}$ with $\alpha \geq \beta > \frac{n-d}{2}$ and $\frac{d}{2\alpha} + \frac{n-d}{2\beta} < 1$, then the error of interpolation approximation $\mathcal{I}_{K,L}$ (3.8) is

$$\begin{aligned} |u - \mathcal{I}_{K,L}u|_{\mu,\nu} &\lesssim (K^{-\alpha} + L^{-\beta})(K^\mu + L^\nu)|u|_{\alpha,\beta}, \\ \|u - \mathcal{I}_{K,L}u\|_{\mu,\nu} &\lesssim (K^{-\alpha} + L^{-\beta})(K^\mu + L^\nu)\|u\|_{\alpha,\beta}, \end{aligned}$$

for $\mu \in [0, \alpha]$, $\nu \in [0, \beta]$.

Proof. The proof is in Appendix C. \square

REMARK 3.4. According to the convergence result of IWFPM interpolation presented above, it is evident that for some special quasiperiodic functions with distinct regularities along different directions (means that the gap between α and β is huge), our proposed hyperparallelogram index set $\mathcal{K}_{K,L}$ can achieve the consistent convergence effect by adjusting K and L .

4. Application to quasiperiodic Schrödinger eigenproblems (QSEs). In this section, we apply IWFPM to solve 1D, 2D, and 3D QSEs. Consider the eigenproblems with quasiperiodic Schrödinger operator $H : \mathcal{C}^2(\mathbb{R}^d) \rightarrow \mathcal{C}(\mathbb{R}^d)$, $d = 1, 2, 3$ as

$$(4.1) \quad Hu(\mathbf{x}) := -\frac{1}{2}\Delta u(\mathbf{x}) + v(\mathbf{x})u(\mathbf{x}) = Eu(\mathbf{x}),$$

where $v(\mathbf{x})$ is a quasiperiodic potential, the eigenfunction $u(\mathbf{x})$ is the normalized wavefunction, and the eigenvalue E represents the corresponding energy.

4.1. IWFPM discretization. Suppose that $U(\mathbf{y})$ and $V(\mathbf{y})$ are the parent functions of $u(\mathbf{x})$ and $v(\mathbf{x})$, respectively. Let $\tilde{\mathbf{U}}$ be the Fourier coefficients vector of $U(\mathbf{y})$ on the index set $\mathcal{K}_{K,L}$, and $\mathbf{V} = \text{diag}(V(\mathbf{y}))_{\mathbf{y} \in \mathcal{G}_{K,L}}$. Then, by the discretization of IWFPM, solving QSE (4.1) can be expressed as finding an eigenpair $(E, \tilde{\mathbf{U}})$ such that

$$\tilde{\mathbf{H}}\tilde{\mathbf{U}} := \mathbf{\Lambda}\tilde{\mathbf{U}} + \mathbf{F}\mathbf{V}\mathbf{F}^{-1}\tilde{\mathbf{U}} = E\tilde{\mathbf{U}}, \quad \mathbf{\Lambda} = \frac{1}{2} \text{diag}(\|\mathbf{P}\mathbf{k}\|^2)_{\mathbf{k} \in \mathcal{K}_{K,L}},$$

where \mathbf{F} is the discrete Fourier transform corresponding to IWFPD defined by (3.9). To solve this eigenvalue problem in matrix form, we employ the locally optimal block preconditioned conjugate gradient (LOBPCG) method [23], with convergence error 1.0e-10 and initial vector $\mathbf{e}_1 = (1, 0, \dots, 0)^T$. The preconditioner selected in LOBPCG method is

$$(4.2) \quad \mathbf{M} = \operatorname{argmin}_{\mathbf{D} \in \mathcal{D}} \|\tilde{\mathbf{H}}\mathbf{D} - \mathbf{I}\|_F = \operatorname{diag}(\tilde{h}_{11}/\|\tilde{\mathbf{H}}\mathbf{e}_1\|_2^2, \dots, \tilde{h}_{NN}/\|\tilde{\mathbf{H}}\mathbf{e}_N\|_2^2),$$

where $N = 2^n K^d L^{n-d}$ is the size of matrix $\tilde{\mathbf{H}}$, and \tilde{h}_{ii} is the i -th diagonal element of $\tilde{\mathbf{H}}$, $i = 1, \dots, N$. $\|\cdot\|_F$ means the Frobenius norm and \mathcal{D} is the set of all diagonal matrices of order N . More details about this preconditioner can refer to [21].

4.2. Numerical experiments. Now we present the numerical results obtained by IWFPD and demonstrate the performance by comparing with PM. All algorithms are coded by Matlab 2022b. The computations for 1D and 2D QSEs are carried out on a workstation with an Inter Core 2.10 GHz CPU and 16 GB RAM. IT and CPU represent the required iterations and the CPU time (in seconds), respectively. $\text{DOF} := 2^n K^d L^{n-d}$ denotes the degrees of freedom. In this section, we consistently present the calculation results of the minimum eigenvalue E_0 and the corresponding eigenfunction $u_0(\mathbf{x})$. We observe the eigfunction in grid form as $\mathbf{u}_0 = (u_0(\boldsymbol{\xi}))_{\boldsymbol{\xi} \in \mathcal{G}}$, where \mathcal{G} is a uniform grid on the bounded region $\mathcal{G} = [-5a, 5a]^d$ ($a = 10^{3-d}$) with the step size $h = 0.1$, and normalize it through dividing by the norm of maximal module $\|\mathbf{u}_0\|_\infty$. The probability density of eigenfunction \mathbf{u}_0 is denoted as $\boldsymbol{\rho} := |\mathbf{u}_0|^2$. We use relative errors of E_0 and \mathbf{u}_0 to measure the numerical accuracy

$$E_v = \left| \frac{E_0 - E_0^*}{E_0^*} \right| \quad \text{and} \quad E_f = \|\mathbf{u}_0 - \mathbf{u}_0^*\|_\infty,$$

where E_0^* and \mathbf{u}_0^* are corresponding numerical exact solutions of E_0 and \mathbf{u}_0 , respectively.

EXAMPLE 4.1. Consider 1D QSE (4.1) with potential

$$(4.3) \quad v(x) = v_0[2 - \cos(2\pi x) - \cos(2\pi\alpha x)],$$

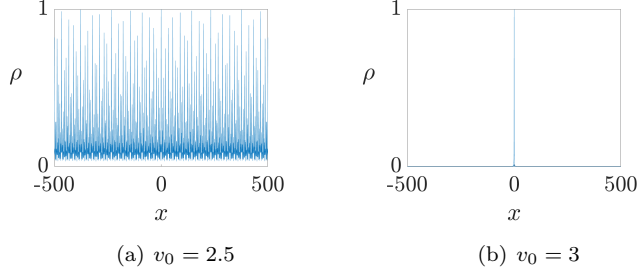
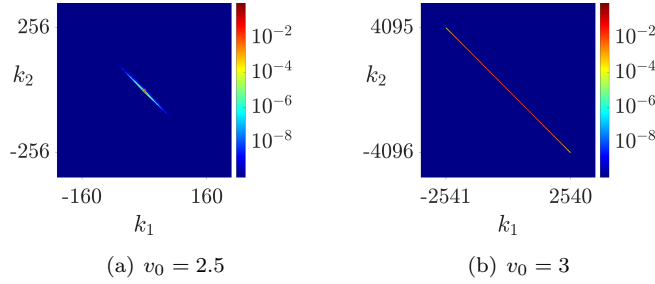
where $v_0 \in \mathbb{R}$, $\alpha = (\sqrt{5} - 1)/2$.

The projection matrix corresponding to (4.3) is $\mathbf{P} = 2\pi(1, \alpha)$, then $v(x)$ can be embedded into the 2D parent function $V(\mathbf{y}) = v_0(2 - \cos y_1 - \cos y_2)$, $\mathbf{y} = (y_1, y_2)^T$. According to (3.1), the hyperparallelogram index set is

$$\mathcal{K}_{K,L} = \{\mathbf{k} = (k_1, k_2)^T \in \mathbb{Z}^2 : k_1 + \alpha k_2 \in [-K, K), k_2 \in [-L, L]\}.$$

This example is worth considering due to the observable phase transition from extended state to localized state as v_0 increases. To verify this, we present the probability density function ρ under the potential (4.3) with different v_0 , as shown in Figure 3. The wavefunction exhibits an extended state when $v_0 = 2.5$, and translates into a localized state when $v_0 = 3$.

Next, we present the generalized Fourier coefficients $\tilde{U}_{\mathbf{k}}$ in Figure 4. It can be observed that the Fourier coefficients $\tilde{U}_{\mathbf{k}}$, whose intensities are larger than 1.0e-8, are mainly concentrated within a narrow parallelogram area. IWFPD method has a natural advantage in solving quasiperiodic problems with such Fourier coefficient distribution. Moreover, compared with the case $v_0 = 2.5$, the concentrated area of

Fig. 3: The probability density function ρ for 1D QSE with potential (4.3).Fig. 4: Distribution of Fourier coefficients $\tilde{U}_{\mathbf{k}}$ for 1D QSE with potential (4.3).

the case $v_0 = 3$ is greatly elongated. Entire size of this concentrated area can reach 5082×8192 . Such a large computing area could be unaffordable for PM. However, by using the parallelogram index set $\mathcal{K}_{K,L}$ with a small K , IWFPM remains a viable approach to efficiently solve this case. To demonstrate the superiority of our algorithm in handling the above two cases, we use both PM and IWFPM to solve this QSE.

Table 1: Condition numbers of $\tilde{\mathbf{H}}$ and $\mathbf{M}\tilde{\mathbf{H}}$ for 1D QSE with potential (4.3) ($v_0 = 2.5$).

DOF		Condition Number					
		$\tilde{\mathbf{H}}$			$\mathbf{M}\tilde{\mathbf{H}}$		
L		200	400	800	200	400	800
$K = 200$	PM	4.72e+05	9.02e+05	2.17e+06	2.24	2.24	2.24
	IWFPM	1.81e+05	1.81e+05	1.81e+05	2.24	2.24	2.24
K		50	100	200	50	100	200
$L = 1600$	PM	4.87e+06	5.35e+06	6.37e+06	2.24	2.24	2.24
	IWFPM	1.15e+04	4.55e+04	1.81e+05	2.24	2.24	2.24

Case 1: $v_0 = 2.5$. First, in Table 1, we give a comparison of the condition numbers of $\tilde{\mathbf{H}}$ before and after preconditioning, to show the effectiveness of the preconditioner \mathbf{M} defined by (4.2). The results show that whether using PM or IWFPM, the condition numbers of $\tilde{\mathbf{H}}$ generally exceed the magnitude of $1.0\text{e}+04$. While after preconditioning, they are remarkably reduced from $>1.0\text{e}+04$ to 2.24.

After using the powerful preconditioning, we next compare the algorithm accuracy

of PM and IWFPm in terms of eigenvalue and eigenfunction errors. To present the tiny errors clearly, we set the calculated eigenvalue E_0^* and eigenfunction \mathbf{u}_0^* of a large-scale system as the numerical exact solution for comparison. Here, E_0^* and \mathbf{u}_0^* are calculated by PM with $K = 640$, $L = 1024$. Table 2 records the errors of eigenvalue E_0 and eigenfunction \mathbf{u}_0 , respectively. The data shows that both PM and IWFPm methods can achieve high accuracy in calculating this example. While, by comparison, it can be seen that under the same L , PM will need a more lager K to achieve the same convergence accuracy compared with IWFPm. For instance, $E_v = 2.84\text{e-}14$ and $E_f = 1.49\text{e-}05$, achieved by using the IWFPm with $K = 5$, require $K = 0.7L = 42$ to be achieved using PM.

Table 2: Errors of PM and IWFPm when solving 1D QSE with potential (4.3) ($v_0 = 2.5$).

		L	20	40	60
E_v	PM	$K = 0.3L$	1.45e-05	7.35e-08	9.42e-10
		$K = 0.5L$	4.60e-07	2.79e-10	4.13e-13
		$K = 0.7L$	5.64e-08	2.69e-11	2.82e-14
	IWFPm	$K = 5$	5.64e-08	2.11e-11	2.84e-14
E_f	PM	$K = 0.3L$	1.11e-01	1.91e-02	2.59e-03
		$K = 0.5L$	3.00e-02	2.05e-03	5.13e-05
		$K = 0.7L$	1.82e-02	4.03e-04	1.49e-05
	IWFPm	$K = 5$	1.82e-02	3.48e-04	1.49e-05

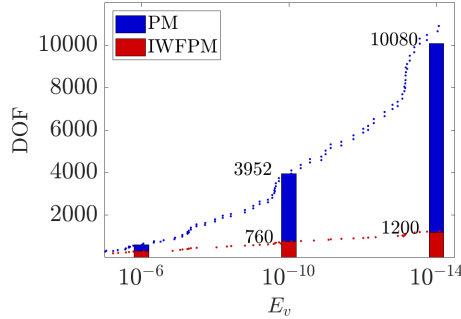


Fig. 5: Required DOFs of PM and IWFPm when they achieve the same accurate E_v for solving 1D QSE with potential (4.3) ($v_0 = 2.5$).

Note that the size of K and L affects the DOFs of the two algorithms, which in turn fundamentally affects their calculation time. Hence, we next present Figure 5 to show the DOFs required by PM and IWFPm when they achieve the same errors of E_0 . It is obvious that as the required accuracy increases, the DOF required for PM rises sharply compared to IWFPm. When $E_v \approx 2.8\text{e-}14$, the DOF of IWFPm is 1200, while the DOF of PM has exceeded 10000. We further compare the computational costs of PM and IWFPm. Table 3 records the ITs and CPU times required by PM and IWFPm when $E_v \approx 2.8\text{e-}14$. It is clear that although the ITs required by the two methods to achieve the same convergence accuracy are basically the same, the CPU time consumed differs by 10.75 times. In conclusion, the above series of comparison

results all demonstrate that IWFPM can greatly improve the calculation efficiency of PM.

Table 3: ITs and CPU times required by PM and IWFPM when solving the 1D QSE with potential (4.3) ($v_0 = 2.5$).

	PM	IWFPM	PM/IWFPM
E_v	2.84e-14	2.82e-14	1.01
DOF	10080	1200	8.40
IT	204	195	1.00
CPU(s)	0.86	0.08	10.75

Case 2: $v_0 = 3$. In this case, the preconditioner \mathbf{M} remains effective. For example, it can reduce the condition number of $\tilde{\mathbf{H}}$ discretized by PM with $K = 640$, $L = 1024$ from 6.3430e+06 to 2.39.

Table 4: Results of PM and IWFPM for solving the 1D QSE with potential (4.3) ($v_0 = 3$).

	IWFPM				PM	PM/IWFPM
E_v	9.78e-06	2.45e-06	6.03e-07	1.42e-07	1.44e-07	1.01
E_f	8.43e-03	3.65e-03	4.16e-04	3.81e-04	3.57e-04	0.94
DOF	4096	8192	16384	32768	2621440	80
IT	1147	2140	4092	6871	7656	1.11
CPU(s)	0.57	1.72	6.08	22.87	3057.75	133.70

Table 4 records the results of PM and IWFPM for solving the eigenvalue E_0 and eigenfunction \mathbf{u}_0 . Here, the numerical exact solutions E_0^* and \mathbf{u}_0^* are obtained by IWFPM with $K = 10$, $L = 4096$. The reason why we not use PM to obtain a true numerical solution is that the excessively large calculation area in this case makes PM unaffordable. As we can see, IWFPM can achieve the same accuracy as PM with much fewer DOF, which means less computational cost. For example, when the error $E_0 \approx 1.4\text{e-}07$, the DOF of IWFPM is 32768, while PM is 2621440. The ratio of CPU time consumed by the two methods is 133.70.

EXAMPLE 4.2. Consider 2D QSE (4.1) with potential

$$(4.4) \quad v(\mathbf{x}) = 4 - [\cos(\beta x_1) + 2 \cos(\beta x_2) + \cos(\beta x_1 \cos \theta + \beta x_2 \sin \theta)],$$

where $\mathbf{x} = (x_1, x_2)^T$, $\beta \in \mathbb{R}$, $\theta \in (0, 2\pi)$.

The projection matrix of $v(\mathbf{x})$ is

$$\mathbf{P} = \beta \begin{pmatrix} 1 & 0 & \cos \theta \\ 0 & 1 & \sin \theta \end{pmatrix},$$

and the corresponding parent function is

$$V(\mathbf{y}) = 4 - (\cos y_1 + 2 \cos y_2 + \cos y_3), \quad \mathbf{y} = (y_1, y_2, y_3)^T.$$

The parallelogram index set $\mathcal{K}_{K,L}$ defined by (3.1) is

$$\mathcal{K}_{K,L} = \left\{ \mathbf{k} = (k_1, k_2, k_3)^T \in \mathbb{Z}^3 : k_1 + k_3 \cos \theta \in [-K, K], k_2 + k_3 \sin \theta \in [-K, K], k_3 \in [-L, L] \right\}.$$

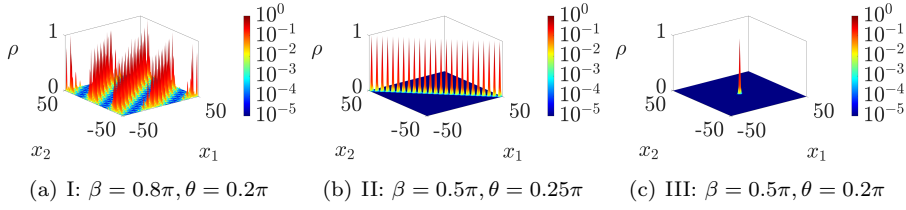


Fig. 6: Probability density function ρ for 2D QSE with potential (4.4).

Figure 6 shows probability density function ρ under the potential (4.4) with different parameters β and θ . Among them, Figure 6(a) shows a 2D extended state and Figure 6(c) shows a 2D localized state. The phase transition between the two states arises from β plays a dominant role in interfering in the degree of localization of the wave function. While some special values of θ can bring periodicity to the wave function. As shown in Figure 6(b), when $\beta = 0.5\pi$, $\theta = 0.25\pi$, the ρ exhibits extended state along the line $x_1 + x_2 = 0$ and localized state in the orthogonal direction.

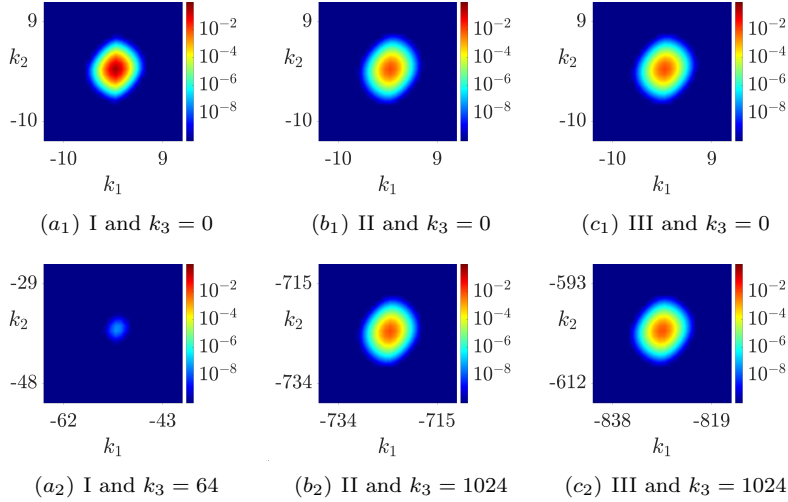


Fig. 7: Slices of the Fourier coefficient $\tilde{U}_{\mathbf{k}}$ for the 2D QSE with potential (4.4) (I: $\beta = 0.8\pi$, $\theta = 0.2\pi$; II: $\beta = 0.5\pi$, $\theta = 0.25\pi$; III: $\beta = 0.5\pi$, $\theta = 0.2\pi$).

Next, we consider the concentrated area of the Fourier coefficient $\tilde{U}_{\mathbf{k}}$ ($\gg 1.0\text{e-}8$) under the potential (4.4) with different parameters. Since the reciprocal space of this example is 3D, we need to use slices to show the area edge with respect to the k_3 direction. Similar to Example 4.1, localized states require a higher DOF than extended states. In the following, we use IWFPM to solve the above mentioned three quantum states and compare the results with PM.

Case 1: I: $\beta = 0.8\pi$, $\theta = 0.2\pi$. In this example, we also use the preconditioner \mathbf{M} to reduce the condition number of $\tilde{\mathbf{H}}$. When addressing the $\tilde{\mathbf{H}}$ discretized by PM with $K = 40$, $L = 50$, \mathbf{M} can reduce the condition number from $1.18\text{e}+04$ to 2.70.

Table 5 records the errors of eigenvalue E_0 and eigenfunction \mathbf{u}_0 , respectively. Here, the numerical exact solution E_0^* and \mathbf{u}_0^* are calculated by IWFPM when $K = 10$, $L = 160$. Compared with PM, IWFPM exhibits higher-order convergence under a small scale of K . Specifically, when $K = 6$, $L = 20$, the error E_v of IWFPM reaches $4.53\text{e-}08$, while the error of PM has not reach $7.51\text{e-}05$. To achieve the same magnitude of error, PM would need $K = 16$, $L = 20$.

Table 5: Errors of PM and IWFPM when solving 2D QSE with potential (4.4) (I: $\beta = 0.8\pi$, $\theta = 0.2\pi$).

		L	20	30	40	50
E_v	PM	$K = 0.4L$	$7.51\text{e-}05$	$2.55\text{e-}06$	$6.21\text{e-}08$	$1.83\text{e-}09$
		$K = 0.6L$	$2.55\text{e-}06$	$1.48\text{e-}08$	$8.60\text{e-}11$	$1.65\text{e-}12$
		$K = 0.8L$	$7.35\text{e-}08$	$9.88\text{e-}11$	$3.85\text{e-}13$	$1.11\text{e-}15$
	IWFPM	$K = 6$	$4.53\text{e-}08$	$3.09\text{e-}11$	$1.84\text{e-}13$	$1.11\text{e-}15$
E_f	PM	$K = 0.4L$	$1.55\text{e-}01$	$2.58\text{e-}02$	$3.48\text{e-}03$	$7.99\text{e-}04$
		$K = 0.6L$	$2.58\text{e-}02$	$1.94\text{e-}03$	$2.22\text{e-}04$	$3.46\text{e-}05$
		$K = 0.8L$	$3.81\text{e-}03$	$2.35\text{e-}04$	$1.43\text{e-}05$	$1.18\text{e-}06$
	IWFPM	$K = 6$	$3.12\text{e-}03$	$1.67\text{e-}04$	$1.00\text{e-}05$	$1.09\text{e-}06$

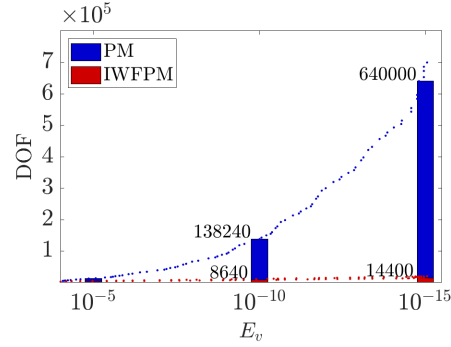


Fig. 8: Required DOFs by PM and IWFPM when they arrive in the same accurate E_v for solving 2D QSE with potential (4.4) (I: $\beta = 0.8\pi$, $\theta = 0.2\pi$).

Table 6: Comparison of ITs and CPU times spent by PM and IWFPM, when solving the 2D QSE with potential (4.4) (I: $\beta = 0.8\pi$, $\theta = 0.2\pi$) with $E_v \approx 1.1\text{e-}15$.

	PM	IWFPM	PM/IWFPM
E_v	$1.11\text{e-}15$	$1.11\text{e-}15$	1.00
DOF	640000	14400	44.44
IT	227	229	0.99
CPU(s)	25.27	0.39	64.79

We further compare the ITs and CPU times of PM and IWFPM when achieving the same accuracy. First, Figure 8 illustrates the DOFs required by PM and IWFPM when they achieve the same errors of E_0 . Once again, the results underscore that, in comparison to IWFPM, PM exhibits a notable drawback in terms of computational storage. Then, we consider the case when the error is about $1.1\text{e-}15$. The data in

Table 6 shows that although PM and IWFPm have almost the same IT, the difference in DOF is as high as 44 times, which ultimately results in IWFPm taking over 64 times CPU time less than PM.

Case 2: II: $\beta = 0.5\pi$, $\theta = 0.25\pi$ **and III:** $\beta = 0.5\pi$, $\theta = 0.2\pi$. Table 7 and Table 8 presents the errors, ITs, and CPU times of IWFPm and PM for solving the eigenvalue E_0 and eigenfunction u_0 . Here, the numerical exact solution E_0^* and u_0^* are calculated by IWFPm when $K = 10$, $L = 4096$. The data once again shows the high efficiency and accuracy of IWFPm, regardless of whether the wave function solved is a periodic localized state or a localized state. For comparison, when the two methods both achieve the error $E_v \approx 1.5\text{e-}05$, it is apparent that the DOF required by PM is 156 times larger than that needed by IWFPm. As a result, the CPU time consumed by PM is 168 times larger than that by IWFPm.

Table 7: Results of PM and IWFPm for solving the 2D QSE with potential (4.4) (II: $\beta = 0.5\pi$, $\theta = 0.25\pi$).

	IWFPm				PM	PM/IWFPm
E_v	1.51e-05	3.76e-06	9.30e-07	2.22e-07	1.51e-05	1.00
E_f	4.34e-03	1.08e-03	2.88e-04	5.64e-05	4.36e-03	1.00
DOF	65536	131072	262144	524288	10240000	156.25
IT	1873	3538	6726	13133	1653	0.88
CPU(s)	16.98	71.56	264.67	1009.56	3050.37	179.64

Table 8: Results of PM and IWFPm for solving the 2D QSE with potential (4.4) (III: $\beta = 0.5\pi$, $\theta = 0.2\pi$).

	IWFPm				PM	PM/IWFPm
E_v	1.43e-05	3.58e-06	8.85e-07	2.11e-07	1.54e-05	1.08
E_f	9.59e-01	9.01e-01	6.94e-01	1.75e-01	9.61e-01	1.00
DOF	65536	131072	262144	524288	10240000	156.25
IT	1911	3612	6870	13426	1653	0.87
CPU(s)	18.53	77.50	274.81	1025.83	3111.78	167.93

EXAMPLE 4.3. Consider 3D QSE (4.1) with potential

$$(4.5) \quad v(\mathbf{x}) = 6 - [\cos(\beta x_1) + \cos(\beta x_2) + \cos(\beta x_3) + \cos(\beta x_1 \cos \theta + \beta x_2 \sin \theta) \\ + \cos(-\beta x_1 \sin \theta + \beta x_2 \cos \theta) + \cos(\beta \alpha x_3)]$$

where $\mathbf{x} = (x_1, x_2, x_3)^T$, $\beta \in \mathbb{R}$, $\theta = 0.2\pi$, $\alpha = (\sqrt{5} - 1)/2$.

The projection matrix of $v(\mathbf{x})$ is

$$\mathbf{P} = \beta \begin{pmatrix} 1 & 0 & 0 & \cos \theta & -\sin \theta & 0 \\ 0 & 1 & 0 & \sin \theta & \cos \theta & 0 \\ 0 & 0 & 1 & 0 & 0 & \alpha \end{pmatrix},$$

and the corresponding parent function is

$$\mathcal{V}(\mathbf{y}) = 6 - \cos \mathbf{y}, \quad \mathbf{y} = (y_1, \dots, y_6)^T.$$

The spectral point set $\mathcal{K}_{K,L}$ defined by (3.1) is

$$\begin{aligned} \mathcal{K}_{K,L} = \{ \mathbf{k} = (k_1, \dots, k_6)^T \in \mathbb{Z}^6 : & k_1 + k_4 \cos \theta - k_5 \sin \theta \in [-K, K), \\ & k_2 + k_4 \sin \theta + k_5 \cos \theta \in [-K, K), \quad k_3 + k_6 \alpha \in [-K, K), \\ & k_4 \in [-L, L), \quad k_5 \in [-L, L), \quad k_6 \in [-L, L) \}. \end{aligned}$$

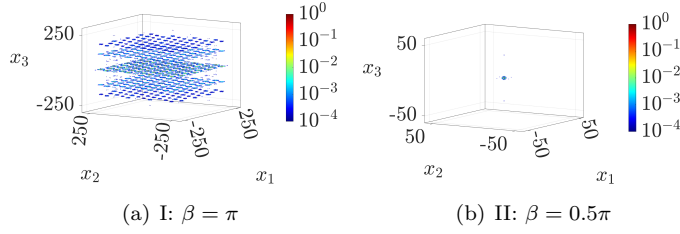


Fig. 9: The probability density function ρ for 3D QSE with potential (4.5).

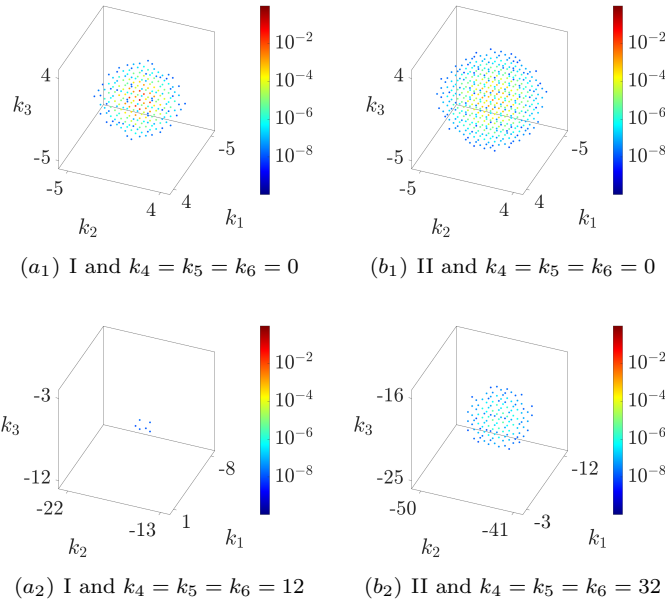


Fig. 10: Slices of the Fourier coefficient $\tilde{U}_{\mathbf{k}}$ for the 3D QSE with potential (4.5) (I: $\beta = \pi$; II: $\beta = 0.5\pi$).

Figure 9 shows the probability density function ρ under the potential (4.5) with different parameters β . When $\beta = \pi$, the wave function diffuses throughout the entire 3D space, which seems to be a 3D extended state. Conversely, when $\beta = 0.5\pi$, the wave function becomes localized at a point in the 3D space, which seems to be a 3D localized state. In this example, we also use the preconditioner \mathbf{M} to reduce the

condition number of $\tilde{\mathbf{H}}$. When addressing the $\tilde{\mathbf{H}}$ discretized by PM with $K = 9$, $L = 10$, \mathbf{M} can reduce the condition number from $8.59\text{e}+03$ to 2.34 .

To show the concentrated distribution of Fourier coefficients within a hyperparallelogram area, we also depict the slices of $\tilde{U}_{\mathbf{k}}$ under the potential (4.5) with different parameters in Figure 10. Clearly, the L required for the case I is less than 12, while the L required for the case II is more than 32. To calculate the case II in a 6D space will bring a huge storage difficulty for PM (DOF exceeding 10^8).

Table 9: Results of IWFPMP for solving the 3D QSE with potential (4.5) (I: $\beta = \pi$; II: $\beta = 0.5\pi$).

$K = 5$	E_v		E_f	
L	I	II	I	II
10	6.82e-04	4.08e-03	2.88e-04	3.55e-02
20	1.58e-04	9.91e-04	1.94e-04	4.84e-03
30	4.34e-05	2.71e-04	9.32e-05	2.21e-03

However, IWFPMP enables the calculation of this problem by significantly optimizing the DOF. Table 9 records the results of IWFPMP for solving the eigenvalue E_0 and eigenfunction \mathbf{u}_0 . Here, the numerical exact solutions E_0^* and \mathbf{u}_0^* of E_0 and \mathbf{u}_0 are obtained by IWFPMP with $K = 5$, $L = 40$. The data show that IWFPMP can achieve convergence effects when calculating 3D QSE with (4.5), regardless of whether the solution belongs to extended state or localized state.

5. Conclusion and outlook. This paper is concerned with developing a new algorithm for solving arbitrary dimensional global quasiperiodic systems. Based on PM, we propose the IWFPMP, which further utilizes the concentrated distribution of Fourier coefficients to filter out relevant spectral points using an irrational window. Moreover, a corresponding index-shift transform is designed to make the Fast Fourier Transform available. The corresponding convergence analysis and computational cost of IWFPMP are also given. We apply IWFPMP to 1D, 2D, and 3D QSEs to demonstrate its accuracy and efficiency. An efficient diagonal preconditioner is also designed for the discrete QSEs to significantly reduce condition number. For both extended and localized quantum states, IWFPMP exhibits a significant computational advantage over PM.

The proposed method opens avenues for further research in several directions. Firstly, given the widespread existence of the observed spectral point distribution feature, it is imperative to apply the IWFPMP to a broader range of quasiperiodic systems to demonstrate its applicability. Secondly, the convergence analysis of quasiperiodic eigenproblems differs from conventional numerical analysis, as the Hilbert space for describing potential energy functions and eigenfunctions is entirely different. New fundamental theories of numerical analysis are needed to describe this problem, and we plan to explore this in our future work. Thirdly, we will extend the application of our method to more quasiperiodic systems, aiming to discover exotic phenomena and even unveil new physical laws.

REFERENCES

- [1] P. W. Anderson, *Absence of diffusion in certain random lattices*, Physical Review, **109**(1958), 1492.

- [2] A. Avila and S. Jitomirskaya, *The ten martini problem*, Annals of Mathematics, **170**(2009), 303–342.
- [3] A. Avila, *Global theory of one-frequency Schrödinger operators*, Acta Mathematica, **215**(2015), 1–54.
- [4] A. Avila, J. You, and Q. Zhou, *Sharp phase transitions for the almost Mathieu operator*, Duke Mathematical Journal, **166**(2017), 2697–2718.
- [5] M. Baake and U. Grimm, *Aperiodic order*, vol. 1, Cambridge University Press, 2013.
- [6] I. Babuška and J. Osborn, *Eigenvalue problems*, Elsevier, 1991.
- [7] H. Bohr, *Almost periodic functions*, Courier Dover Publications, 2018.
- [8] D. Cao, J. Shen, and J. Xu, *Computing interface with quasiperiodicity*, Journal of Computational Physics, **424**(2021), 109863.
- [9] B. Deissler, M. Zaccanti, G. Roati, C. D’Errico, M. Fattori, M. Modugno, G. Modugno, and M. Inguscio, *Delocalization of a disordered bosonic system by repulsive interactions*, Nature Physics, **6**(2010), 354–358.
- [10] Z. Gao, Z. Xu, Z. Yang, F. Ye, *Pythagoras Superposition Principle for Localized Eigenstates of 2D Moiré Lattices*, Physical Review A, **108**(2023), 013513.
- [11] Z. Gao, Z. Xu, and Z. Yang, *Reduced projection method for quasiperiodic Schrödinger eigenvalue problems*, (2023), arXiv:2309.09238.
- [12] L. Ge, S. Jitomirskaya, J. You, and Q. Zhou, *Multiplicative Jensen’s formula and quantitative global theory of one-frequency Schrödinger operators*, (2023), arXiv:2306.16387.
- [13] L. Grafakos, *Classical fourier analysis*, vol. 2, Springer, 2008.
- [14] M. Z. Hasan and C. L. Kane, *Colloquium: topological insulators*, Reviews of Modern Physics, **82**(2010), 3045.
- [15] D. R. Hofstadter, *Energy levels and wave functions of Bloch electrons in rational and irrational magnetic fields*, Physical Review B, **14**(1976), 2239.
- [16] K. Jiang and P. Zhang, *Numerical methods for quasicrystals*, Journal of Computational Physics, **256**(2014), 428–440.
- [17] K. Jiang, J. Tong, P. Zhang, and A.-C. Shi, *Stability of two-dimensional soft quasicrystals in systems with two length scales*, Physical Review E, **92**(2015), 042159.
- [18] K. Jiang, S. Li, and P. Zhang, *On the approximation of quasiperiodic functions with Diophantine frequencies by periodic functions*, (2023), arXiv:2304.04334.
- [19] K. Jiang, S. Li, and J. Zhang, *High-accuracy numerical methods and convergence analysis for Schrödinger equation with incommensurate potentials*, (2023), arXiv:2312.16462.
- [20] K. Jiang, S. Li, and P. Zhang, *Numerical methods and analysis of computing quasiperiodic systems*, SIAM Journal on Numerical Analysis, **62**(2024), 353–375.
- [21] K. Jiang, M. Li, J. Zhang, and L. Zhang, *Projection method for quasiperiodic elliptic equations and application to quasiperiodic homogenization*, (2024), In preparation.
- [22] S. Y. Jitomirskaya, *Metal-insulator transition for the almost Mathieu operator*, Annals of Mathematics, (1999), 1159–1175.
- [23] A. V. Knyazev, *Toward the optimal preconditioned eigensolver: locally optimal block preconditioned conjugate gradient method*, SIAM Journal on Scientific Computing, **23**(2001), 517–541.
- [24] X. Li and K. Jiang, *Numerical simulation for quasiperiodic quantum dynamical systems*, Journal on Numerical Methods and Computer Applications, **42**(2021), 3.
- [25] Y. Meyer, *Algebraic numbers and harmonic analysis*, Elsevier, 2000.
- [26] M. Modugno, *Exponential localization in one-dimensional quasi-periodic optical lattices*, New Journal of Physics, **11**(2009), 033023.
- [27] R. Penrose, *The role of aesthetics in pure and applied mathematical research*, Bulletin of the Institute of Mathematics and Its Applications, **10** (1974), 266–271.
- [28] H. Poincaré, *Sur le problème des trois corps et les équations de la dynamique*, Acta Mathematica, **13**(1890), A3–A270.
- [29] G. Roati, C. D’Errico, L. Fallani, M. Fattori, C. Fort, M. Zaccanti, G. Modugno, M. Modugno, and M. Inguscio, *Anderson localization of a non-interacting Bose-Einstein condensate*, Nature, **453**(2008), 895–898.
- [30] S. D. Sarma, S. He, and X. Xie, *Mobility edge in a model one-dimensional potential*, Physical Review Letters, **61**(1988), 2144.
- [31] D. Shechtman, I. Blech, D. Gratias, and J. W. Cahn, *Metallic phase with long-range orientational order and no translational symmetry*, Physical Review Letters, **53**(1984), 1951.
- [32] J. Shen, T. Tang, and L.-L. Wang, *Spectral methods: algorithms, analysis and applications*, vol. 41, Springer Science & Business Media, 2011.
- [33] B. Simon, *Schrödinger operators in the twenty-first century*, Mathematical Physics, **2000**(2000), 283–288.

- [34] G. W. Stewart, *A Krylov–Schur algorithm for large eigenproblems*, SIAM Journal on Matrix Analysis and Applications, **23**(2002), 601–614.
- [35] S. Stützer, Y. Plotnik, Y. Lumer, P. Titum, N. H. Lindner, M. Segev, M. C. Rechtsman, and A. Szameit, *Photonic topological Anderson insulators*, Nature, **560**(2018), 461–465.
- [36] A. Sutton and R. Balluffi, *Interfaces in crystalline materials*, Clarendon Press, 1995.
- [37] D. J. Thouless, M. Kohmoto, M. P. Nightingale, and M. den Nijs, *Quantized Hall conductance in a two-dimensional periodic potential*, Physical Review Letters, **49**(1982), 405.
- [38] Y. Wang, X. Xia, L. Zhang, H. Yao, S. Chen, J. You, Q. Zhou, and X.-J. Liu, *One-dimensional quasiperiodic mosaic lattice with exact mobility edges*, Physical Review Letters, **125**(2020), 196604.
- [39] P. Wang, Y. Zheng, X. Chen, C. Huang, Y. V. Kartashov, L. Torner, V. V. Konotop, and F. Ye, *Localization and delocalization of light in photonic moiré lattices*, Nature, **577**(2020), 42–46.
- [40] T. Wang, H. Chen, A. Zhou, Y. Zhou, and D. Massatt, *Convergence of the planewave approximations for quantum incommensurate systems*, (2022), arXiv:2204.00994.
- [41] C. Wang, F. Liu, and H. Huang, *Effective model for fractional topological corner modes in quasicrystals*, Physical Review Letters, **129**(2022), 056403.
- [42] P. Zhang and X. Zhang, *An efficient numerical method of Landau-Brazovskii model*, Journal of Computational Physics, **227**(2008), 5859–5870.
- [43] Y. Zhou, H. Chen, and A. Zhou, *Plane wave methods for quantum eigenvalue problems of incommensurate systems*, Journal of Computational Physics, **384**(2019), 99–113.

Appendix A. Proof of Lemma 3.1.

Proof. We only prove the equivalence $|u|_{\alpha,\beta} \simeq |u|_{\alpha} + |U|_{\mathcal{H}^{\beta}}$, since the other is similar. First, it is easy to obtain $|u|_{\alpha,\beta} \lesssim |u|_{\alpha} + |U|_{\mathcal{H}^{\beta}}$ since

$$\begin{aligned} |u|_{\alpha,\beta}^2 &= \sum_{\mathbf{k} \in \mathbb{Z}^n} (\|\mathbf{k}_I + \mathbf{Q}\mathbf{k}_{II}\|^{2\alpha} + \|\mathbf{k}_{II}\|^{2\beta}) |\hat{U}_{\mathbf{k}}|^2 \\ &= \sum_{\mathbf{k} \in \mathbb{Z}^n} (\|\mathbf{P}_I^{-1}\|^{2\alpha} \|\mathbf{P}\mathbf{k}\|^{2\alpha} + \|\mathbf{k}\|^{2\beta}) |\hat{U}_{\mathbf{k}}|^2 \\ &\lesssim \sum_{\mathbf{k} \in \mathbb{Z}^n} \|\mathbf{P}\mathbf{k}\|^{2\alpha} |\hat{U}_{\mathbf{k}}|^2 + \sum_{\mathbf{k} \in \mathbb{Z}^n} \|\mathbf{k}\|^{2\beta} |\hat{U}_{\mathbf{k}}|^2. \end{aligned}$$

Next, we prove the converse $|u|_{\alpha} + |U|_{\mathcal{H}^{\beta}} \lesssim |u|_{\alpha,\beta}$. It can be divided into two parts: $|u|_{\alpha} \lesssim |u|_{\alpha,\beta}$ and $|U|_{\mathcal{H}^{\beta}} \lesssim |u|_{\alpha,\beta}$. The former can be obtained naturally because

$$|u|_{\alpha}^2 = \sum_{\mathbf{k} \in \mathbb{Z}^n} \|\mathbf{P}\mathbf{k}\|^{2\alpha} |\hat{U}_{\mathbf{k}}|^2 = \sum_{\mathbf{k} \in \mathbb{Z}^n} \|\mathbf{P}_I\|^{2\alpha} \|\mathbf{k}_I + \mathbf{Q}\mathbf{k}_{II}\|^{2\alpha} |\hat{U}_{\mathbf{k}}|^2.$$

For the latter

$$|U|_{\mathcal{H}^{\beta}}^2 = \sum_{\mathbf{k} \in \mathbb{Z}^n} \|\mathbf{k}\|^{2\beta} |\hat{U}_{\mathbf{k}}|^2 = \sum_{\mathbf{k} \in \mathbb{Z}^n} (\|\mathbf{k}_I\|^{2\beta} + \|\mathbf{k}_{II}\|^{2\beta}) |\hat{U}_{\mathbf{k}}|^2,$$

then we only need to focus on $\|\mathbf{k}_I\|^{2\beta}$. We discuss it in three cases. The first case is $\mathbf{k}_{II} = 0$, and it is obvious

$$\|\mathbf{k}_I\|^{2\beta} = \|\mathbf{k}_I + \mathbf{Q}\mathbf{k}_{II}\|^{2\beta} \leq \|\mathbf{k}_I + \mathbf{Q}\mathbf{k}_{II}\|^{2\alpha}.$$

The second case is $\mathbf{k}_{II} \neq 0$ and $\|\mathbf{k}_I + \mathbf{Q}\mathbf{k}_{II}\| < 1$, and it yields

$$\|\mathbf{k}_I\| \leq \|\mathbf{k}_I + \mathbf{Q}\mathbf{k}_{II}\| + \|\mathbf{Q}\mathbf{k}_{II}\| < 1 + \|\mathbf{Q}\mathbf{k}_{II}\| \leq (1 + \|\mathbf{Q}\|) \|\mathbf{k}_{II}\|.$$

The third case is $\mathbf{k}_{II} \neq 0$ and $\|\mathbf{k}_I + \mathbf{Q}\mathbf{k}_{II}\| \geq 1$, and we have

$$\|\mathbf{k}_I\| \leq \|\mathbf{k}_I + \mathbf{Q}\mathbf{k}_{II}\| + \|\mathbf{Q}\| \|\mathbf{k}_{II}\|,$$

which yields

$$\|\mathbf{k}_I\|^{2\beta} \leq C_1 (\|\mathbf{k}_I + \mathbf{Q}\mathbf{k}_{II}\|^{2\beta} + \|\mathbf{k}_{II}\|^{2\beta}) \leq C_1 (\|\mathbf{k}_I + \mathbf{Q}\mathbf{k}_{II}\|^{2\alpha} + \|\mathbf{k}_{II}\|^{2\beta}),$$

where C_1 is a constant independent of \mathbf{k} . The above inequalities can lead to

$$\|\mathbf{k}\|^{2\beta} \leq C_2 (\|\mathbf{k}_I + \mathbf{Q}\mathbf{k}_{II}\|^{2\alpha} + \|\mathbf{k}_{II}\|^{2\beta}),$$

and so $|U|_{\mathcal{H}^\beta} \lesssim |u|_{\alpha,\beta}$. \square

Appendix B. Proof of Lemma 3.2.

Proof. First of all, it is easy to obtain the following inequality

$$\begin{aligned} |u - \mathcal{P}_{K,L}u|_{\mu,\nu}^2 &= \sum_{\mathbf{k} \in \mathbb{Z}^n \setminus \mathcal{K}_{K,L}} (\|\mathbf{k}_I + \mathbf{Q}\mathbf{k}_{II}\|^{2\mu} + \|\mathbf{k}_{II}\|^{2\nu}) |\hat{U}_{\mathbf{k}}|^2 \\ &\leq (a_1 + a_2) + (a_3 + a_4), \end{aligned}$$

where

$$\begin{aligned} a_1 &= \sum_{\mathbf{k}_{II} \in \mathbb{Z}^{n-d}} \sum_{\|\mathbf{k}_I + \mathbf{Q}\mathbf{k}_{II}\|_\infty \geq K} \|\mathbf{k}_I + \mathbf{Q}\mathbf{k}_{II}\|^{2\mu} |\hat{U}_{\mathbf{k}}|^2, \\ a_2 &= \sum_{\|\mathbf{k}_{II}\|_\infty \geq L} \sum_{\|\mathbf{k}_I + \mathbf{Q}\mathbf{k}_{II}\|_\infty < K} \|\mathbf{k}_I + \mathbf{Q}\mathbf{k}_{II}\|^{2\mu} |\hat{U}_{\mathbf{k}}|^2 \\ a_3 &= \sum_{\mathbf{k}_I \in \mathbb{Z}^d} \sum_{\|\mathbf{k}_{II}\|_\infty \geq L} \|\mathbf{k}_{II}\|^{2\nu} |\hat{U}_{\mathbf{k}}|^2, \\ a_4 &= \sum_{\|\mathbf{k}_{II}\|_\infty < L} \sum_{\|\mathbf{k}_I + \mathbf{Q}\mathbf{k}_{II}\|_\infty \geq K} \|\mathbf{k}_{II}\|^{2\nu} |\hat{U}_{\mathbf{k}}|^2, \end{aligned}$$

and $\|\mathbf{m}\|_\infty = \max_{1 \leq j \leq n'} \{m_j\}$ for $\mathbf{m} \in \mathbb{R}^{n'}$. Using the equivalence of vector norms, we have

$$\begin{aligned} a_1 &= \sum_{\mathbf{k}_{II} \in \mathbb{Z}^{n-d}} \sum_{\|\mathbf{k}_I + \mathbf{Q}\mathbf{k}_{II}\|_\infty \geq K} \|\mathbf{k}_I + \mathbf{Q}\mathbf{k}_{II}\|^{2\mu-2\alpha} \|\mathbf{k}_I + \mathbf{Q}\mathbf{k}_{II}\|^{2\alpha} |\hat{U}_{\mathbf{k}}|^2 \\ &\leq K^{2\mu-2\alpha} \sum_{\mathbf{k}_{II} \in \mathbb{Z}^{n-d}} \sum_{\|\mathbf{k}_I + \mathbf{Q}\mathbf{k}_{II}\|_\infty \geq K} \|\mathbf{P}_I^{-1}\|^{2\alpha} \|\mathbf{P}\mathbf{k}\|^{2\alpha} |\hat{U}_{\mathbf{k}}|^2 \\ &\lesssim K^{2\mu-2\alpha} |u|_\alpha^2, \\ a_2 &\leq K^{2\mu} \sum_{\|\mathbf{k}_{II}\|_\infty \geq L} \sum_{\|\mathbf{k}_I + \mathbf{Q}\mathbf{k}_{II}\|_\infty < K} \|\mathbf{k}_{II}\|^{-2\beta} \|\mathbf{k}_{II}\|^{2\beta} |\hat{U}_{\mathbf{k}}|^2 \lesssim K^{2\mu} L^{-2\beta} |U|_{\mathcal{H}^\beta}^2, \\ a_3 &= \sum_{\mathbf{k}_I \in \mathbb{Z}^d} \sum_{\|\mathbf{k}_{II}\|_\infty \geq L} \|\mathbf{k}_{II}\|^{2\nu-2\beta} \|\mathbf{k}_{II}\|^{2\beta} |\hat{U}_{\mathbf{k}}|^2 \leq L^{2\nu-2\beta} |U|_{\mathcal{H}^\beta}^2, \\ a_4 &\leq L^{2\nu} \sum_{\|\mathbf{k}_{II}\|_\infty < L} \sum_{\|\mathbf{k}_I + \mathbf{Q}\mathbf{k}_{II}\|_\infty \geq K} \|\mathbf{P}\mathbf{k}\|^{-2\alpha} \|\mathbf{P}\mathbf{k}\|^{2\alpha} |\hat{U}_{\mathbf{k}}|^2 \\ &= L^{2\nu} \|\mathbf{P}_I\|^{-2\alpha} \sum_{\|\mathbf{k}_{II}\|_\infty < L} \sum_{\|\mathbf{k}_I + \mathbf{Q}\mathbf{k}_{II}\|_\infty \geq K} \|\mathbf{k}_I + \mathbf{Q}\mathbf{k}_{II}\|^{-2\alpha} \|\mathbf{P}\mathbf{k}\|^{2\alpha} |\hat{U}_{\mathbf{k}}|^2 \\ &\lesssim L^{2\nu} K^{-2\alpha} |u|_\alpha^2. \end{aligned}$$

Combining the above four equations, we can obtain the estimate of $|u - \mathcal{P}_{K,L}u|_{\mu,\nu}$ in the original proposition. Following the similar proof, we can also obtain the estimate of $\|u - \mathcal{P}_{K,L}u\|_{\mu,\nu}$. \square

Appendix C. Proof of Theorem 3.4.

Proof. From the definition of discrete inner product (3.7), it is easy to prove that the Fourier basis functions satisfy the following discrete orthogonality

$$(C.1) \quad \langle \varphi_{\mathbf{k}}, \varphi_{\mathbf{k}'} \rangle_{K,L} = \begin{cases} 1, & \mathbf{k} - \mathbf{k}' \in \mathcal{Z}_{K,L}, \\ 0, & \text{otherwise,} \end{cases}$$

where

$$\mathcal{Z}_{K,L} := \{\mathbf{m} = (\mathbf{m}_I, \mathbf{m}_{II})^T \in \mathbb{Z}^n : \mathbf{m}_I/(2K) \in \mathbb{Z}^d, \mathbf{m}_{II}/(2L) \in \mathbb{Z}^{n-d}\}.$$

This discrete orthogonality leads to the following aliasing formula

$$(C.2) \quad \tilde{u}_{\mathbf{k}} = \left\langle \sum_{l \in \mathbb{Z}^n} \hat{U}_l \varphi_{Pl}, \varphi_{P\mathbf{k}} \right\rangle_{K,L} = \sum_{\mathbf{m} \in \mathbb{Z}^n} \hat{U}_{(\mathbf{k}_I + 2K\mathbf{m}_I, \mathbf{k}_{II} + 2L\mathbf{m}_{II})},$$

for any $\mathbf{k} \in \mathcal{K}_{K,L}$. Thus,

$$\mathcal{P}_{K,L}u(\mathbf{y}) - \mathcal{I}_{K,L}u(\mathbf{y}) = \sum_{\mathbf{k} \in \mathcal{K}_{K,L}} \varphi_{\mathbf{k}}(\mathbf{y}) \sum_{\mathbf{m} \in \mathbb{Z}^n \setminus \{\mathbf{0}_n\}} \hat{U}_{(\mathbf{k}_I + 2K\mathbf{m}_I, \mathbf{k}_{II} + 2L\mathbf{m}_{II})},$$

where $\mathbf{0}_n$ denotes the n -dimensional zero vector. Let

$$g(\mathbf{k}, \mathbf{m}) = \|\mathbf{k}_I + 2K\mathbf{m}_I + \mathbf{Q}(\mathbf{k}_{II} + 2L\mathbf{m}_{II})\|^{2\alpha} + \|\mathbf{k}_{II} + 2L\mathbf{m}_{II}\|^{2\beta}.$$

Note that $g(\mathbf{k}, \mathbf{m}) = 0$ if and only if $\mathbf{k} = \mathbf{m} = 0$, and this is because the column vectors of the projection matrix \mathbf{P} are \mathbb{Q} -linearly independent. Using the Cauchy-Schwarz inequality, we have

$$(C.3) \quad \begin{aligned} & \|\mathcal{P}_{K,L}u - \mathcal{I}_{K,L}u\|_{\mathcal{L}^2}^2 \\ &= \sum_{\mathbf{k} \in \mathcal{K}_{K,L}} \left| \sum_{\mathbf{m} \in \mathbb{Z}^n \setminus \{\mathbf{0}_n\}} \hat{U}_{(\mathbf{k}_I + 2K\mathbf{m}_I, \mathbf{k}_{II} + 2L\mathbf{m}_{II})} \right|^2 \\ &= \sum_{\mathbf{k} \in \mathcal{K}_{K,L}} \left| \sum_{\mathbf{m} \in \mathbb{Z}^n \setminus \{\mathbf{0}_n\}} g(\mathbf{k}, \mathbf{m})^{-1/2} g(\mathbf{k}, \mathbf{m})^{1/2} \hat{U}_{(\mathbf{k}_I + 2K\mathbf{m}_I, \mathbf{k}_{II} + 2L\mathbf{m}_{II})} \right|^2 \\ &\leq \sum_{\mathbf{k} \in \mathcal{K}_{K,L}} \sum_{\mathbf{m} \in \mathbb{Z}^n \setminus \{\mathbf{0}_n\}} g(\mathbf{k}, \mathbf{m})^{-1} \sum_{l \in \mathbb{Z}^n \setminus \{\mathbf{0}_n\}} g(\mathbf{k}, l) |\hat{U}_{(\mathbf{k}_I + 2Kl_I, \mathbf{k}_{II} + 2Ll_{II})}|^2. \end{aligned}$$

Next, we consider the series

$$\sum_{\mathbf{m} \in \mathbb{Z}^n \setminus \{\mathbf{0}_n\}} g(\mathbf{k}, \mathbf{m})^{-1} = \sum_{\substack{\mathbf{m}_I \in \mathbb{Z}^d \\ \mathbf{m}_{II} \neq \mathbf{0}_{n-d}}} g(\mathbf{k}, \mathbf{m})^{-1} + \sum_{\substack{\mathbf{m}_I \neq \mathbf{0}_d \\ \mathbf{m}_{II} = \mathbf{0}_{n-d}}} g(\mathbf{k}, \mathbf{m})^{-1} = b_1 + b_2.$$

Since $\mathbf{k}_{II} \in [-L, 1-L, \dots, L]^{n-d}$, we have

$$\|\mathbf{k}_{II} + 2L\mathbf{m}_{II}\|^{2\beta} \geq L^{2\beta} \|\mathbf{m}_{II}\|^{2\beta}.$$

For fixed \mathbf{m}_{II} , there exists a unique \mathbf{m}'_I such that

$$\mathbf{k}_I + 2K\mathbf{m}'_I + \mathbf{Q}(\mathbf{k}_{II} + 2L\mathbf{m}_{II}) \in [-K, 1-K, \dots, K]^d,$$

and it is obvious $\mathbf{m}'_I = \mathbf{0}_d$ if $\mathbf{m}_{II} = \mathbf{0}_{n-d}$. Then,

$$\begin{aligned} & \|\mathbf{k}_I + 2K\mathbf{m}_I + \mathbf{Q}(\mathbf{k}_{II} + 2L\mathbf{m}_{II})\|^{2\alpha} \\ &= \|2K(\mathbf{m}_I - \mathbf{m}'_I) + \mathbf{k}_I + 2K\mathbf{m}'_I + \mathbf{Q}(\mathbf{k}_{II} + 2L\mathbf{m}_{II})\|^{2\alpha} \\ &\geq K^{2\alpha} \|(\mathbf{m}_I - \mathbf{m}'_I)\|^{2\alpha}. \end{aligned}$$

Thus,

$$\begin{aligned} b_1 &= \sum_{\mathbf{m}_I \in \mathbb{Z}^d} \sum_{\mathbf{m}_{II} \neq \mathbf{0}_{n-d}} (\|\mathbf{k}_I + 2K\mathbf{m}_I + \mathbf{Q}(\mathbf{k}_{II} + 2L\mathbf{m}_{II})\|^{2\alpha} + \|\mathbf{k}_{II} + 2L\mathbf{m}_{II}\|^{2\beta})^{-1} \\ &\leq \sum_{\mathbf{m}_I \in \mathbb{Z}^d} \sum_{\mathbf{m}_{II} \neq \mathbf{0}_{n-d}} (K^{2\alpha} \|(\mathbf{m}_I - \mathbf{m}'_I)\|^{2\alpha} + L^{2\beta} \|\mathbf{m}_{II}\|^{2\beta})^{-1} \\ &\leq \max\{K^{-2\alpha}, L^{-2\beta}\} \sum_{\mathbf{m}_I \in \mathbb{Z}^d} \sum_{\mathbf{m}_{II} \neq \mathbf{0}_{n-d}} (\|\mathbf{m}_I\|^{2\alpha} + \|\mathbf{m}_{II}\|^{2\beta})^{-1}, \\ b_2 &\leq \sum_{\mathbf{m}_I \neq \mathbf{0}_d} \|\mathbf{k}_I + 2K\mathbf{m}_I + \mathbf{Q}\mathbf{k}_{II}\|^{-2\alpha} \leq K^{-2\alpha} \sum_{\mathbf{m}_I \neq \mathbf{0}_d} \|\mathbf{m}_I\|^{-2\alpha}. \end{aligned}$$

Combining the above two inequalities, we have

$$\sum_{\mathbf{m} \in \mathbb{Z}^n \setminus \{\mathbf{0}_n\}} g(\mathbf{k}, \mathbf{m})^{-1} \lesssim (K^{-2\alpha} + L^{-2\beta}) \sum_{\mathbf{m}_I \neq \mathbf{0}_d} \sum_{\mathbf{m}_{II} \neq \mathbf{0}_{n-d}} (\|\mathbf{m}_I\|^{2\alpha} + \|\mathbf{m}_{II}\|^{2\beta})^{-1}.$$

The sufficient condition for the convergence series $\sum_{\mathbf{m}_I \neq \mathbf{0}_d} \|\mathbf{m}_I\|^{-2\alpha} \sum_{\mathbf{m}_{II} \neq \mathbf{0}_{n-d}} \|\mathbf{m}_{II}\|^{-2\beta}$, $\alpha > d/2$ and $\beta > (n-d)/2$, can be easily obtained by Hölder's inequality. Moreover, the condition $d/2\alpha + (n-d)/2\beta < 1$ implies that there exists $\alpha' > d$ and $\beta' > n-d$ such that

$$\frac{\alpha'}{2\alpha} + \frac{\beta'}{2\beta} = 1,$$

and by Young's inequality, we have

$$\sum_{\mathbf{m}_I \neq \mathbf{0}_d} \sum_{\mathbf{m}_{II} \neq \mathbf{0}_{n-d}} (\|\mathbf{m}_I\|^{2\alpha} + \|\mathbf{m}_{II}\|^{2\beta})^{-1} \leq \sum_{\mathbf{m}_I \neq \mathbf{0}_d} \sum_{\mathbf{m}_{II} \neq \mathbf{0}_{n-d}} \|\mathbf{m}_I\|^{-\alpha'} \|\mathbf{m}_{II}\|^{-\beta'},$$

which is obviously convergent. The convergence of the series yields

$$\sum_{\mathbf{m} \in \mathbb{Z}^n \setminus \{\mathbf{0}_n\}} g(\mathbf{k}, \mathbf{m})^{-1} \lesssim (K^{-2\alpha} + L^{-2\beta}).$$

Therefore, it follows (C.3) that

$$\begin{aligned} \|\mathcal{P}_{K,L}u - \mathcal{I}_{K,L}u\|_{\mathcal{L}^2}^2 &\lesssim (K^{-2\alpha} + L^{-2\beta}) \sum_{\mathbf{k} \in \mathcal{K}_{K,L}} \sum_{\mathbf{l} \in \mathbb{Z}^n \setminus \{\mathbf{0}_n\}} g(\mathbf{k}, \mathbf{l}) |\hat{U}_{(\mathbf{k}_I + 2K\mathbf{l}_I, \mathbf{k}_{II} + 2L\mathbf{l}_{II})}|^2 \\ &\leq (K^{-2\alpha} + L^{-2\beta}) |u|_{\alpha, \beta}^2. \end{aligned}$$

Moreover,

$$\begin{aligned} |\mathcal{P}_{K,L}u - \mathcal{I}_{K,L}u|_{\mu, \nu}^2 &= \sum_{\mathbf{k} \in \mathcal{K}_{K,L}} (\|\mathbf{k}_I + \mathbf{Q}\mathbf{k}_{II}\|^{2\mu} + \|\mathbf{k}_{II}\|^{2\nu}) |\hat{U}_{\mathbf{k}} - \tilde{u}_{\mathbf{k}}|^2 \\ &\leq (K^{2\mu} + L^{2\nu}) \|\mathcal{P}_{K,L}u - \mathcal{I}_{K,L}u\|_{\mathcal{L}^2}^2 \\ &\lesssim (K^{-2\alpha} + L^{-2\beta}) (K^{2\mu} + L^{2\nu}) |u|_{\alpha, \beta}^2. \end{aligned}$$

Thus, from [Corollary 3.3](#), we have

$$\begin{aligned} |u - \mathcal{I}_{K,L}u|_{\mu,\nu}^2 &\leq |u - \mathcal{P}_{K,L}u|_{\mu,\nu}^2 + |\mathcal{P}_{K,L}u - \mathcal{I}_{K,L}u|_{\mu,\nu}^2 \\ &\lesssim (K^{-2\alpha} + L^{-2\beta})(K^{2\mu} + L^{2\nu})|u|_{\alpha,\beta}^2. \end{aligned}$$

Similarly, we can also obtain

$$\|u - \mathcal{I}_{K,L}u\|_{\mu,\nu}^2 \lesssim (K^{-2\alpha} + L^{-2\beta})(K^{2\mu} + L^{2\nu})\|u\|_{\alpha,\beta}^2.$$

The original proposition is established. \square